^{31}P magnetization transfer measurements of Pi->ATP flux in exercising human muscle

Alison Sleigh[1,2], David B. Savage[3], Guy B. Williams[1], David Porter[4], T. Adrian Carpenter[1], Kevin M. Brindle[5,6], Graham J. Kemp[7,8]

[1] Wolfson Brain Imaging Centre, University of Cambridge School of Clinical Medicine, Cambridge Biomedical Campus, Cambridge, CB2 0QQ, U.K

[2] National Institute for Health Research / Wellcome Trust Clinical Research Facility at Cambridge University Hospitals NHS Foundation Trust, Cambridge Biomedical Campus, Cambridge, CB2 0QQ, U.K.

[3] University of Cambridge Metabolic Research Laboratories, Wellcome Trust-Medical Research Council Institute of Metabolic Science, Cambridge Biomedical Campus, Cambridge, CB2 0QQ, U.K.

[4] Fraunhofer MEVIS, Institute for Medical Image Computing, Universitaetsallee 29, 28359 Bremen, Germany.

[5] Department of Biochemistry, University of Cambridge, Cambridge, CB2 1GA, U.K.

[6] Cancer Research UK Cambridge Institute, Li Ka Shing Centre, University of Cambridge, Cambridge Biomedical Campus, Cambridge, CB2 0RE, U.K.

[7] Magnetic Resonance and Image Analysis Research Centre, University of Liverpool, Liverpool, L69 3GE, U.K.

[8] Department of Musculoskeletal Biology and MRC – Arthritis Research UK Centre for Integrated research into Musculoskeletal Ageing, Institute of Ageing and Chronic Disease, University of Liverpool, Liverpool, L69 3GA, U.K.

Running title: ST measurements of Pi->ATP flux in exercising human muscle

Keywords: ^{31}P magnetization transfer; saturation transfer; Pi<->ATP exchange; exercising muscle.

Corresponding author: A. Sleigh, Wolfson Brain Imaging Centre, University of Cambridge, Box 65 Addenbrooke's Hospital, Cambridge Biomedical Campus, Cambridge, CB2 0QQ, U.K. (e-mail: as626@wbic.cam.ac.uk)

During production: Phone: +44(0)1223 746460. Fax: +44(0)1223 331826

Abstract (250 words)

Fundamental criticisms have been made over the use of ^{31}P-MRS magnetization transfer estimates of Pi->ATP flux (V_{Pi-ATP}) in human resting skeletal muscle for assessing mitochondrial function. Although the discrepancy in the magnitude of V_{Pi-ATP} is now acknowledged, little is known about its metabolic determinants. Here we use a novel protocol to measure V_{Pi-ATP} in human exercising muscle for the first time.

Steady state V_{Pi-ATP} was measured at rest and over a range of exercise intensities, and compared with suprabasal oxidative ATP synthesis rates estimated from the initial rates of post-exercise phosphocreatine resynthesis (V_{ATP}). We define a 'surplus' Pi->ATP flux as the difference between V_{Pi-ATP} and V_{ATP}.

The coupled reactions catalyzed by the glycolytic enzymes glyceraldehyde 3-phosphate dehydrogenase (GAPDH) and phosphoglycerate kinase (PGK) have been shown to catalyze measurable exchange between ATP and Pi in some systems and have been suggested to be responsible for this surplus flux. Surplus V_{Pi-ATP} did not change between rest and exercise, even though the concentrations of [Pi] and [ADP], which are substrates for GAPDH and PGK, respectively, increased as expected. However, involvement of these enzymes is suggested by correlations between absolute and surplus Pi->ATP flux, both at rest and during exercise, and the intensity of the phosphomonoester peak in the ^{31}P NMR spectrum. This peak includes contributions from sugar phosphates in the glycolytic pathway and changes in its intensity may indicate changes in downstream glycolytic intermediates, including 3-phosphoglycerate, which has been shown to influence the exchange between ATP and Pi catalyzed by GAPDH and PGK.

INTRODUCTION

^{31}P-MRS magnetization transfer measurements of flux between Pi and ATP (Pi->ATP), called here 'saturation transfer' (ST), have been widely implemented for the putative assessment of mitochondrial function in skeletal muscle. In 2008 Kemp drew attention to the striking fact that in resting muscle ST is an order of magnitude larger than the net rate of oxidative ATP synthesis that it was claimed to measure, a discrepancy too large to be compensated by the use of relative data presentations such as test/control or post/pre ratios (13). This, and the separate point that a resting flux has no straightforward relationship to metabolic capacity (13, 16), have stimulated much recent debate over the interpretation of this measurement (2, 3, 11, 16, 27, 29, 35).

This discrepancy between ST and known or inferred rates of oxidative ATP synthesis (which we call here the 'surplus' ST rate) in skeletal muscle is usually attributed to a rapid near equilibrium Pi<->ATP exchange catalyzed by the glycolytic enzymes glyceraldehyde 3-phosphate dehydrogenase (GAPDH; EC 1.2.1.12) and phosphoglycerate kinase (PGK; EC 2.7.2.3). Some early ST measurements of Pi->ATP flux in *Saccharomyces cerevisiae* (5, 6, 9) provided evidence for a GAPDH/PGK-mediated exchange contribution. In addition, an *in vitro* study (8) showed that this GAPDH/PGK couple could, with simulated levels of enzymes and substrates, catalyze sufficient Pi-ATP exchange to explain data obtained in glucose-perfused rat heart. This was confirmed subsequently by Kingsley-Hickman et al. (20) in intact perfused rat myocardium, where they manipulated glycolysis over a range of oxygen consumption rates. GAPDH and PGK activities are similar in human and rat heart and in rat skeletal and human intercostal muscle (31, 32). Although GAPDH activity is lower in human skeletal muscle, as compared to rat skeletal muscle (106±28 versus 294±36 U/g tissue), it is still similar or greater than that of rat heart (31, 32).

Another potential explanation for a surplus Pi->ATP flux relates to a mitochondrial Pi-ATP exchange. LaNoue et al. (21) used ^{33}P-radiolabelled tracers in isolated rat liver and heart mitochondria to demonstrate a significant ATP->Pi flux, (i.e. in the reverse direction to ATP synthesis), and thus unidirectional Pi->ATP rates in excess of the net ATP synthesis rate. In the transition from zero to maximal net ATP synthesis (in moving from state 4 to 3 respiration) the Pi->ATP flux doubled, while the reverse ATP->Pi flux decreased by >90%. Brindle et al. (30) also provided evidence for a mitochondrial Pi-ATP exchange in vivo using ST measurements in yeast, where they removed the glycolytic exchange catalyzed by GAPDH and PGK by lowering PGK expression using an attenuated promoter. Subtraction of the net glycolytic Pi->ATP flux, estimated from measurements of glucose consumption, showed that overexpression of the adenosine nucleotide translocase (ANT) significantly increased the Pi->ATP flux determined using ST measurements.

Other explanations proposed for the anomalously large Pi-ATP flux, such as rapidly-exchanging small pools of metabolites (2), remain speculative. In skeletal muscle the literature has generally been interpreted as favoring a glycolytic Pi-ATP exchange mediated by the GAPDH/PGK couple (16, 27, 35), although it has been speculated (3, 11, 30) that in resting muscle, with its low respiration rates, mitochondrial-associated Pi-ATP exchange may become more prominent (21).

To investigate the determinants of this flux *in vivo*, we set out to define the effects of varying oxidative ATP synthesis rates on the ST measurements in human skeletal muscle, which has been the main organ of interest in recent ST studies. There have been few studies of ST over a range of respiration rates: in stimulated rat hindlimb muscle (7), in lamb myocardium *in vivo* (26) and perfused rat myocardium (20), and in rat brain under varying levels of anesthesia (10). The rat hindlimb study (7) has been incorrectly cited (12, 22, 37) as supporting the

validity of the *resting* ST as a measure of oxidative ATP synthesis. This study showed only that the Pi->ATP flux in the *stimulated* muscle was not very different to the rates of net oxidative ATP synthesis observed in other studies using similar experimental preparations and concluded that a glycolytic exchange contribution could not be ruled out, particularly in resting muscle. The lamb and rat myocardium studies (20, 26) found that the 'surplus' Pi->ATP flux remained approximately constant, or decreased, with increasing oxidative ATP synthesis rate. A retrospective comparison of the rat hindlimb results (7) with a range of published non-ST data showed a similar picture (13). In the brain study (10) oxygen consumption was not measured. To study this relationship directly we designed a protocol to measure the steady-state rates of Pi->ATP flux over a range of exercise intensities in human skeletal muscle, and compared these with immediate post-exercise rates of phosphocreatine (PCr) resynthesis, which are a measure of the suprabasal end-exercise mitochondrial oxidative ATP synthesis rate (15). We hypothesized that the surplus Pi->ATP flux was due to the exchange catalyzed by GAPDH and PGK and that this would remain unchanged, or decrease, with increasing oxidative ATP synthesis rate.

METHODS

Participants. Each participant provided written informed consent and all studies were conducted in accordance with the Declaration of Helsinki. Ethical approval was granted by the UK National Research Ethics Service. Eleven healthy adult volunteers (7 male, 4 female) were recruited, with mean ± SEM age 29.4 ± 2.8 y and BMI 22.8 ± 0.9 kg/m^2. Exclusion criteria were standard magnet contraindications, diabetes mellitus or cardiovascular disease,

inability to understand protocol instructions, smokers, and those taking medication or supplements known to affect energy metabolism.

Protocol. Participants were recruited into group A or B, except one volunteer who entered both groups. Group A consisted of nine volunteers who undertook a single ^{31}P-MRS scan with a workload predetermined using a fraction of their previously measured maximum voluntary contraction force. In order to test the feasibility of this exercise protocol in a variety of participants and over a range of ATP turnover rates this fraction was varied between the volunteers. The three participants in group B undertook 4 ^{31}P-MRS scans on different days; the workload varied between visits, yielding sufficient PCr depletion (for measurement of PCr resynthesis) at low workloads, whilst maintaining the exercise tolerability and minimal acidification at higher workloads.

On a pre-scanning visit, volunteers' maximum voluntary contraction force was measured using a leg dynamometer (set to the same initial angle of exercise as in the MR scanner), and they were shown an instruction video and given the opportunity to practice to ensure they were comfortable with the full in-scanner exercise protocol.

^{31}P-MRS. Studies used a Siemens MAGNETOM 3T Verio (Erlangen, Germany) scanner, and each ^{31}P-MRS scan consisted of resting and exercising ST measurements as well as assessment of post-exercise PCr recovery kinetics (Figure 1). The volunteers were positioned supine and a 6 cm diameter surface coil (RAPID Biomedical, Rimpar, Germany) attached and located to their right rectus femoris muscle (which was a location that gave the maximal PCr depletion/workload ratio). Precise coil relocation for participants in group B was obtained by using approximate anatomical distances and then accurately by 3D fasciae landmarks. An MR-compatible weight was attached to the right ankle (33) to provide the predetermined workload.

Resting ST measurement. The Pi magnetization was measured in the presence of selective saturation of the γ-ATP resonance (SAT) and compared with a control where the irradiation frequency was placed symmetrical to the Pi peak (CONT), using a 1.32ms BIR-4 adiabatic excitation (34) placed symmetrically between Pi and γ-ATP. TR = 24s, receiver bandwidth (rBW) = 2500 Hz, and number of acquisitions (NA) = 48 for each SAT/CONT. The T_1 of Pi with saturation of the γ-ATP resonance (T_1') was measured using an inversion recovery (IR) pulse sequence (7 TI's between 9-10000ms, effective TR (TR_{eff}) = 6s, NA = 12-20). TI was defined as the time between the inversion and subsequent excitation pulse, and TR_{eff} as the time between the excitation and subsequent inversion pulse. IR data were acquired in blocks which had the same TI, and the first spectrum of each group was eliminated. A fully relaxed spectrum was used to determine metabolite concentrations (NA = 12).

Exercising ST measurement. Figure 1 outlines the exercising ST protocol. Knee extensions were performed (0.5 Hz) and spectra (TR = 2 s) acquired to ensure steady state was reached prior to the ST acquisitions. A soft target was attached to the apex of the scanner bore to prevent participant hyperextension, inhibit waning and aid in maintaining steady state. For the ST measurements triggered headphone instructions gave warning and then instructed the participant to be still during the excitation and subsequent acquisition; any noncompliance resulted in exclusion of that spectrum. Two minutes of exercise preceded the first useable SAT spectrum and they were considered not to be in steady state if their average [PCr] at time = 80 s differed by >2 standard deviations of the end of exercise [PCr] (Figure 1). To avoid significant acidification and to increase tolerability of the protocol, the exercise was split into two bouts (shaded regions in Figure 1). Due to the potential for lengthening of the Pi T_1 upon exercise (24), exercising ST parameters were similar to resting ST but with TR = 34 s, NA = 8 for each SAT/CONT; 5 TI's, NA = 6-15 for the T_1 measurement; and a TR of 44s and NA = 4 for the metabolite spectra.

175 *Post-exercise PCr recovery kinetics.* Ten spectra (TR 2s) were obtained, which ensured that a
176 steady state magnetization had been reached (Figure 1), prior to cessation of exercise and
177 acquisition of spectra of the recovery kinetics (TR = 2s, NA = 150). The PCr recovery rate
178 constant, k_{PCr} , was found using a two parameter monoexponential fit, as described previously
179 (25, 33). The suprabasal mitochondrial oxidative ATP synthesis rate was calculated from the
180 immediate end of exercise rates of PCr resynthesis (V_{ATP}), which were calculated as V_{ATP} =
181 k_{PCr}.[PCr $_{depleted}$], where [PCr $_{depleted}$] was determined as the difference between resting and
182 exercising [PCr] from the fully relaxed metabolite spectra.

183 *^{31}P-MRS analysis.* All spectra were analyzed in jMRUI (23), phased and fitted to Lorentzian
184 line shapes using the AMARES (36) algorithm with prior knowledge relating to resonant
185 frequencies, j-coupling patterns and relative amplitudes. Unlike the resting measurements, no
186 averaging took place during exercise acquisitions and the SAT and CONT individual spectra
187 were fitted (Figure 2), thereby allowing for any change in the Pi chemical shift over time. IR
188 spectra were averaged for each TI prior to fitting. The γ-ATP resonance from the
189 corresponding resting or exercising metabolite spectra was used for calculation of metabolite
190 concentrations, assuming an [ATP] of 8.2 mM (17). The intracellular pH was determined
191 from the chemical shift of inorganic phosphate relative to PCr (1) and the free concentration
192 of ADP was calculated using established methods (1), assuming a total creatine pool of 42.5
193 mM (17). Due to the nonconventional line shapes of the phosphomonoester (PME)
194 resonances, [PME] was determined by integration techniques. This involved using the
195 averaged metabolite spectra and applying an optimized line broadening, equivalent to that of
196 0.75*(line width of one singlet of the γ-ATP resonance doublet), prior to integration of the
197 PME (5.9-7.5ppm) and γ-ATP resonances using the cut and weigh method. The Levenberg-
198 Marquardt fitting algorithm within MATLAB (The MathWorks, Natick, MA, USA) was used
199 to determine the T_1' of Pi from a two parameter monoexponential fit, where Mo was fixed

(from the SAT spectrum at rest and from 'Mo for IR' (Figure 1) when exercising). The first order rate constant (k') was determined according to the equation of Forsen and Hoffman: $k' = [(M_o - M_z)/M_o](1/T_1')$ and the Pi->ATP flux ($V_{Pi\text{-}ATP}$) by multiplication of k' by the concentration of cytosolic Pi. The exercising $V_{Pi\text{-}ATP}$ component above the canonical net rate of oxidative ATP synthesis ('Surplus' $V_{Pi\text{-}ATP}$), was calculated as $V_{Pi\text{-}ATP} - V_{ATP}$, where V_{ATP} was taken as the immediate end of exercise PCr resynthesis rate. As V_{ATP} reflects the rate of suprabasal oxidative ATP synthesis, resting $V_{Pi\text{-}ATP}$ was taken as the equivalent resting surplus $V_{Pi\text{-}ATP}$ measure. The rate constant for post-exercise PCr resynthesis, k_{PCr}, was taken as a measure of muscle mitochondrial capacity (15).

Statistics. Statistical analysis was performed in IBM SPSS Statistics 21 (IBM Inc., Armonk, NY, USA), with a two-tailed significance set at $p < 0.05$. A paired-samples t-test was used to test for significant differences between resting and exercising conditions, using one data pair per person. Spearman's correlation analysis was used to test for significant correlations, since this required fewer assumptions that could be violated. Tests for significant correlations were performed using all datasets from Group A and Group B volunteers, as well as by averaging multiple scans from Group B to give one data point per person. Quantitative data are expressed as mean ± SEM.

RESULTS

All participants completed the exercise protocol, and were fully compliant with the exercise instructions, resulting in no spectral exclusions. One scan (a group B volunteer) was lost due to broadband amplifier hardware failure and for another scan (a group A volunteer) the ST

223 data were lost due to an incorrect saturation frequency. One participant in group B on their
224 final visit declined to provide a resting ST measure but completed the exercise protocol, and
225 another participant (group A) failed to reach the steady-state exercise conditions and their ST
226 exercise data were excluded. All remaining data were used.

227 Figure 2 illustrates the consistency of the steady-state exercise conditions and the changes in
228 metabolite signals during saturation of the γ-ATP resonance in a representative individual.

229 Figure 3 shows typical saturation transfer spectra and inversion recovery plots obtained at rest
230 and during steady-state exercise.

231 Table 1 shows mean rest and exercise values of key ^{31}P MRS measures. The overall mean
232 fractional PCr depletion at steady-state exercise was 25±3 % (n = 20), and the mean post-
233 exercise PCr recovery rate constant (k_{PCr}) was 1.86±0.16 min^{-1} (n = 11, one k_{PCr} value per
234 person). The mean change in pH_i at the end of exercise bout 1, compared with resting
235 conditions, was -0.051±0.016 (n = 20). Splitting of the Pi peak only occurred in one
236 individual in group A, who also had the lowest exercise pH_i and the highest exercising $V_{Pi\text{-}ATP}$
237 of 39 mM/min, and in this individual the two Pi resonances were fitted and then summed.

238 Resting $V_{Pi\text{-}ATP}$ did not correlate significantly with resting [Pi], [ADP], or [H^+] (all $p>0.2$, n =
239 18, or $p>0.5$, n = 10 averaging multiple scans from Group B).

240 Figure 4 compares $V_{Pi\text{-}ATP}$ during exercise with the immediate end-of-exercise rate of
241 suprabasal oxidative ATP synthesis, measured as the initial PCr recovery rate (V_{ATP}). Figure
242 4A shows the relationship between the two, with the line of identity for comparison; Figure
243 4B replaces the absolute $V_{Pi\text{-}ATP}$ flux with the increment in $V_{Pi\text{-}ATP}$ above the resting value.
244 V_{ATP} correlated significantly with both the exercising $V_{Pi\text{-}ATP}$ ($r = 0.552$, $p = 0.017$, n = 18)
245 (Figure 4A) and the suprabasal increment in $V_{Pi\text{-}ATP}$ ($r = 0.500$, $p = 0.041$, n = 17) (Figure

246 4B), but this fell outside statistical significance when averaging the multiple scans from
247 Group B ($r = 0.65$, $p = 0.058$; $r = 0.567$, $p = 0.112$ respectively, $n = 9$). It is clear that surplus
248 $V_{Pi\text{-}ATP}$ (i.e. $V_{Pi\text{-}ATP} - V_{ATP}$, the vertical distance above the line of identity in Figure 4A) does
249 not, on average, change over this range. Using all data points, exercising surplus $V_{Pi\text{-}ATP}$ was
250 not correlated with exercising [Pi], [ADP], or $[H^+]$ (all $p>0.4$, $n = 18$), but was correlated with
251 exercising [Pi] when averaging the multiple scans from Group B ($p = 0.02$, $n = 9$).

252 Figure 5 shows this work rate-invariance for surplus $V_{Pi\text{-}ATP}$, as the lack of a significant
253 difference ($p = 0.912$, $n = 9$) between resting and exercising surplus $V_{Pi\text{-}ATP}$, as assessed by a
254 paired-samples t-test.

255 Figure 6 examines the relationship between $V_{Pi\text{-}ATP}$ and the concentration of the PMEs. First,
256 resting $V_{Pi\text{-}ATP}$ and resting [PME] were highly correlated ($r = 0.740$, $p<0.001$, $n = 18$) (Figure
257 6A), and also when averaging the multiple scans from Group B ($r = 0.770$, $p = 0.009$, $n = 10$);
258 these correlations remained significant after elimination of a possible outlier at low values.
259 Second, exercising $V_{Pi\text{-}ATP}$ and exercising [PME] were also highly correlated ($r = 0.730$, $p =$
260 0.001, $n = 18$) (Figure 6B) (or $r = 0.867$, $p = 0.002$, $n = 9$ when averaging the multiple scans
261 from Group B). $V_{Pi\text{-}ATP}$ comprises two components: a component due to net oxidative ATP
262 synthesis (V_{ATP}), and a 'surplus'. This correlation of $V_{Pi\text{-}ATP}$ during exercise with [PME]
263 appears more closely related to the surplus exercising $V_{Pi\text{-}ATP}$ ($r = 0.534$, $p = 0.023$, $n = 18$; or
264 $r = 0.65$, $p = 0.058$, $n = 9$) (Figure 6C, grey and black symbols) than the V_{ATP} ($r = 0.261$, $p =$
265 0.295, $n = 18$; or $r = 0.067$, $p = 0.865$, $n = 9$) contribution to exercising $V_{Pi\text{-}ATP}$. Linear
266 regression using both resting and exercising data ($n = 36$) found [PME] to be a significant
267 predictor of surplus $V_{Pi\text{-}ATP}$ ($R^2 = 0.291$, $p = 0.001$). Supplementing [PME] with other
268 measured variables revealed that V_{ATP}, [Pi], and [ADP] were also significant predictors of
269 surplus $V_{Pi\text{-}ATP}$, the models yielding the following results: [PME] and V_{ATP} ($R^2 = 0.572$,

[PME] and V_{ATP} both $p<0.001$); [PME] and [Pi] ($R^2 = 0.467$, [PME] $p<0.001$, [Pi] $p = 0.002$); and [PME] and [ADP] ($R^2 = 0.369$, [PME] $p<0.001$, [ADP] $p = 0.051$). In these models V_{ATP}, [Pi], and [ADP] were all significant negative predictors of surplus $V_{Pi\text{-}ATP}$ and hence had a significant effect in reducing the surplus $V_{Pi\text{-}ATP}$. This can be seen in Figure 6C, where for a given [PME] the surplus $V_{Pi\text{-}ATP}$ appears lower when exercising at high V_{ATP}. The [PME] and V_{ATP} model yielded the highest correlation coefficient, and predicted a surplus $V_{Pi\text{-}ATP} = 4.681 + 5.096[PME] - 0.335V_{ATP}$. When averaging the multiple scans from Group B (n = 19), only [PME] alone ($R^2 = 0.675$, [PME] $p = 0.002$) and [PME] with V_{ATP} were significant predictors ($R^2 = 0.787$, [PME] $p <0.001$ and V_{ATP}, $p = 0.02$). Figure 6C also illustrates the apparent work-rate invariance of surplus $V_{Pi\text{-}ATP}$ between resting and exercising conditions (as in Figure 5), and suggests how this may be the result of the counteracting effects of increasing [PME] and decreasing V_{ATP} on the surplus $V_{Pi\text{-}ATP}$. These relationships appear to underpin some of the variation in Figure 4.

Age correlated significantly with k_{PCr} ($r = -0.679$, $p = 0.022$, $n = 11$), but not with resting $V_{Pi\text{-}ATP}$ ($p = 0.44$). Resting $V_{Pi\text{-}ATP}$ did not correlate with k_{PCr} ($p = 0.347$). Also k_{PCr} was not significantly correlated with exercising $V_{Pi\text{-}ATP}$, its suprabasal increment, or the surplus exercise $V_{Pi\text{-}ATP}$.

DISCUSSION

The novel exercise protocol shown in Figure 1 has allowed ST measurements of steady-state Pi->ATP flux over a range of workloads in human skeletal muscle, with limited acidification. Minimizing acidification is important, for two reasons. First, the relationships between pH, [PCr] and [ADP] imposed by the creatine kinase equilibrium mean that the interpretation of

post-exercise PCr recovery kinetics in terms of mitochondrial function is more straightforward. Specifically, a low pH is associated with slower PCr recovery for reasons that have nothing to do with any change in underlying mitochondrial function (15). Secondly, the use of a non-acidifying exercise protocol limits the contribution of net glycolytic ATP production to the measured Pi->ATP flux. From the known stoichiometry of aerobic glycolysis (4), a reasonable approximation for the aerobic glycolytic rate in C6 units is 1/30 of the rate of ATP synthesis. This is an upper limit because it assumes, unrealistically (28), zero contribution by oxidizing fat. In our experiments the rate of oxidative ATP synthesis is estimated as V_{ATP}, the initial post-exercise rate of PCr resynthesis, and the highest measured value of V_{ATP} (Figure 4) implies, therefore, an aerobic glycolytic rate of only ~1 mM/min, or a net glycolytic ATP production rate of ~2 mM/min. Pyruvate can also be reduced to lactate, instead of being oxidized, and the rate of this can be estimated from the change in pH (14, 18). The average pH decrease was ~0.05 units, which previous studies suggest would drive a H^+ efflux rate of ~0.4 mM/min (19). Consumption of H^+ in the creatine kinase reaction can be ignored since there was no change in steady state [PCr]. Therefore the anaerobic glycolytic ATP production rate is ~0.4 mM/min, representing a net glycolytic ATP production rate of no more than ~2.4 mM/min.

The surplus Pi->ATP flux remained approximately constant (Figures 4 & 5) over the range from rest to the highest workloads undertaken (low to moderate respiration rates). This is consistent with inferences drawn from the stimulated rat hindlimb data (7, 11, 13). Similar invariance was also reported over low to moderate workloads in epinephrine-infused lamb myocardium; however, the fact that in that system Pi and ADP concentrations do not vary with workload (26) complicates meaningful comparison. In partial contrast, in glucose-perfused rat myocardium over moderate to high workloads the surplus Pi->ATP flux appeared to decrease with increasing workload (20).

We also report for the first time the relationships between Pi->ATP flux and PME concentration (Figure 6), which included significant correlations of the [PME] with resting, exercising, and surplus Pi->ATP flux. At rest, as well as at the exercise intensities used in our study, the PME resonance is almost exclusively comprised of sugar phosphates (18), mainly glucose 6-phosphate (~80%) fructose 6-phosphate (~15%) and glucose 1-phosphate. The relationship of Pi->ATP flux with a [PME] that contains major contributions from glycolytic pathway substrates appears to be consistent with a large glycolytic Pi-ATP exchange contribution. GAPDH and PGK catalyze the coupled reaction:

$$GAP + Pi + NAD^+ + ADP \rightleftharpoons NADH + H^+ + 3PG + ATP$$

While there was little change in $[H^+]$ there were substantial increases in [Pi] and [ADP] between rest and exercise, yet the overall surplus Pi->ATP flux remained unchanged (Figure 5). One possible explanation for this is that the Pi <->ATP exchange catalyzed by GAPDH and PGK may be also dependent on the concentration of the downstream glycolytic intermediate [3PG], which would be expected to follow, at least to some extent, the concentration of the sugar phosphates represented by the PME resonance. Experiments with isolated GAPDH and PGK have shown a dependence of the exchange on 3PG concentration (8), although the effects of this are difficult to deconvolve from changes in the equilibrium concentrations of the other substrates of the GAPDH/PGK couple; nevertheless linear regression of the data shows [3PG] to be a significant predictor ($p<0.001$). Another factor relevant to the relationship between Pi->ATP flux and [PME] might be the positive correlation of [PME] with [Pi] found when considering all data points (at rest $p = 0.038$; exercising $p = 0.012$, $n = 18$); however (notwithstanding its purely algebraic contribution; $V_{Pi\text{-}ATP} = k'[Pi]$), resting [Pi] was not significantly correlated with resting Pi->ATP flux, nor exercising [Pi] with exercising surplus Pi->ATP flux ($n = 18$).

342 In this work we have defined the response of $V_{Pi\text{-}ATP}$ in human skeletal muscle to large
343 perturbations in the rate of ATP turnover, and partitioned it into the component due to net
344 oxidative ATP synthesis, and what we have called 'surplus' Pi->ATP flux. The approach
345 taken does not of course allow us to dissect contributions to the latter experimentally,
346 although we have shown that net glycolysis cannot be a significant contribution. However, the
347 correlations and surprising lack of correlations we have observed between fluxes and
348 concentrations allow some mechanistic speculation. Taking the resting and exercising data
349 together, [PME] was a significant positive predictor of surplus Pi->ATP flux. Supplementing
350 [PME], the suprabasal oxidative ATP synthesis rate was also found to be a significant
351 predictor of the surplus flux, but acting in the opposite direction (Figure 6C). The opposing
352 effects of [PME] and V_{ATP} resolve into the overall invariance in surplus Pi->ATP flux
353 between resting and exercising conditions (Figure 5 & 6C), and also explain some of the
354 observed variation in Pi->ATP flux (Figures 4 & 6). As little is known about [3PG] levels in
355 skeletal muscle during exercise, we can only speculate that this may reflect a lower 3PG:PME
356 ratio at higher net glycolytic flux.

357 Reflecting on all potential routes for transfer of magnetization between Pi and ATP, the Pi
358 and γ-ATP resonances can exchange magnetization in the coupled reactions catalyzed by
359 GAPDH and PGK, and possibly also via the ATP synthase (30), and via the unidirectional
360 reactions of net ATP synthesis and breakdown. Net ATP synthesis, leading to direct transfer
361 of magnetization between Pi and ATP, takes place in the reaction catalyzed by the
362 mitochondrial ATP synthase and, indirectly, following net glycolytic flux through the
363 GAPDH and PGK reactions, although we have shown the latter to be insignificant under the
364 conditions of this study. Glycolytic ATP synthesis in the reaction catalyzed by pyruvate
365 kinase will not result in transfer of magnetization between Pi and γ-ATP. Net ATP
366 breakdown, leading to direct transfer of magnetization between ATP and Pi, will take place,

in muscle, predominantly in the reaction catalyzed by the myofibrillar ATPase. All other routes for exchange of magnetization between Pi and the γ-phosphate resonance of ATP, most of which are less direct, are likely to be much slower.

In summary we have demonstrated the feasibility of measuring Pi->ATP flux in human exercising muscle over varying workloads. The 'surplus' Pi->ATP flux (that is, the amount by which it exceeds the known net mitochondrial ATP synthesis rate, estimated here from PCr recovery kinetics) is, on average, unchanged between rest and steady state exercising conditions. This is in agreement with previous indirect inferences from rat skeletal muscle data, but seems surprising if (as commonly believed) the source of the surplus flux is Pi-ATP exchange mediated by the glycolytic enzymes GAPDH and PGK, in view of the substantial changes in [Pi] and [ADP] associated with increasing ATP turnover. However, some involvement of the GAPDH/PGK catalyzed exchange is suggested by the correlations observed between absolute and surplus Pi->ATP flux and [PME] both at rest and during exercise. We speculate that this may be due to downstream changes in [3PG] concentration, which has been shown to influence GAPDH/PGK exchange kinetics in vitro.

ACKNOWLEDGMENTS

We are grateful to all the participants and Victoria Lupson (Wolfson Brain Imaging Centre, Cambridge UK). We thank Dr Craig Buckley (Siemens Healthcare Ltd, UK) and Dr Peter Murgatroyd (Cambridge NIHR/Wellcome Trust Clinical Research Facility, UK) for helpful discussions.

GRANTS

This work was funded by the Clinical Research Infrastructure Grant and the Siemens MAGNETOM 3T Verio scanner is funded by the NIHR via an award to the Cambridge NIHR/Wellcome Trust Clinical Research Facility. DBS is supported by the Wellcome Trust (091551).

DISCLOSURES

No conflicts of interest, financial or otherwise, are declared by the author(s).

AUTHOR CONTRIBUTIONS

A.S., G.J.K. conception and design of research; A.S., D.B.S. performed experiments; A.S. analyzed data; A.S., K.M.B., G.J.K. interpreted results of experiments; A.S., G.B.W., D.P., T.A.C. pulse programming code; A.S. prepared figures; A.S., G.J.K. drafted manuscript; A.S., D.P., K.M.B., G.J.K. edited and revised the manuscript; All authors approved the final version of the manuscript.

REFERENCES

1. **Arnold DL, Matthews PM, and Radda GK**. Metabolic recovery after exercise and the assessment of mitochondrial function in vivo in human skeletal muscle by means of 31P NMR. *Magn Reson Med* 1: 307-315, 1984.
2. **Balaban RS, and Koretsky AP**. Interpretation of 31P NMR saturation transfer experiments: what you can't see might confuse you. Focus on "Standard magnetic resonance-based measurements of the Pi-->ATP rate do not index the rate of oxidative phosphorylation in cardiac and skeletal muscles". *Am J Physiol Cell Physiol* 301: C12-15, 2011.
3. **Befroy DE, Rothman DL, Petersen KF, and Shulman GI**. 31P-magnetization transfer magnetic resonance spectroscopy measurements of in vivo metabolism. *Diabetes* 61: 2669-2678, 2012.
4. **Brand MD**. The efficiency and plasticity of mitochondrial energy transduction. *Biochem Soc Trans* 33: 897-904, 2005.
5. **Brindle KM**. 31P NMR magnetization-transfer measurements of flux between inorganic phosphate and adenosine 5'-triphosphate in yeast cells genetically modified to overproduce phosphoglycerate kinase. *Biochemistry* 27: 6187-6196, 1988.
6. **Brindle KM**. 31P Nuclear magnetic resonance saturation transfer measurements of flux between inorganic phosphate and ATP in yeast cells over producing phosphoglycerate kinase *Biochemical Society transactions* 14: 1265, 1986.
7. **Brindle KM, Blackledge MJ, Challiss RA, and Radda GK**. 31P NMR magnetization-transfer measurements of ATP turnover during steady-state isometric muscle contraction in the rat hind limb in vivo. *Biochemistry* 28: 4887-4893, 1989.
8. **Brindle KM, and Radda GK**. 31P-NMR saturation transfer measurements of exchange between Pi and ATP in the reactions catalysed by glyceraldehyde-3-phosphate dehydrogenase and phosphoglycerate kinase in vitro. *Biochim Biophys Acta* 928: 45-55, 1987.
9. **Campbell-Burk SL, Jones KA, and Shulman RG**. 31P NMR saturation-transfer measurements in Saccharomyces cerevisiae: characterization of phosphate exchange reactions by iodoacetate and antimycin A inhibition. *Biochemistry* 26: 7483-7492, 1987.
10. **Du F, Zhu XH, Zhang Y, Friedman M, Zhang NY, Ugurbil K, and Chen W**. Tightly coupled brain activity and cerebral ATP metabolic rate. *Proceedings of the National Academy of Sciences of the United States of America* 105: 6409-6414, 2008.
11. **From AH, and Ugurbil K**. Standard magnetic resonance-based measurements of the Pi-->ATP rate do not index the rate of oxidative phosphorylation in cardiac and skeletal muscles. *Am J Physiol Cell Physiol* 301: C1-11, 2011.
12. **Kacerovsky M, Brehm A, Chmelik M, Schmid AI, Szendroedi J, Kacerovsky-Bielesz G, Nowotny P, Lettner A, Wolzt M, Jones JG, and Roden M**. Impaired insulin stimulation of muscular ATP production in patients with type 1 diabetes. *J Intern Med* 269: 189-199, 2011.
13. **Kemp GJ**. The interpretation of abnormal 31P magnetic resonance saturation transfer measurements of Pi/ATP exchange in insulin-resistant skeletal muscle. *Am J Physiol Endocrinol Metab* 294: E640-642; author reply E643-644, 2008.
14. **Kemp GJ**. Muscle Studies by 31P MRS. *eMagRes* 4: 525-534, 2015.
15. **Kemp GJ, Ahmad RE, Nicolay K, and Prompers JJ**. Quantification of skeletal muscle mitochondrial function by 31P magnetic resonance spectroscopy techniques: a quantitative review. *Acta Physiol* 213: 107-144, 2015.
16. **Kemp GJ, and Brindle KM**. What do magnetic resonance-based measurements of Pi->ATP flux tell us about skeletal muscle metabolism? *Diabetes* 61: 1927-1934, 2012.

17. **Kemp GJ, Meyerspeer M, and Moser E**. Absolute quantification of phosphorus metabolite concentrations in human muscle in vivo by 31P MRS: a quantitative review. *NMR Biomed* 20: 555-565, 2007.
18. **Kemp GJ, Roussel M, Bendahan D, Le Fur Y, and Cozzone PJ**. Interrelations of ATP synthesis and proton handling in ischaemically exercising human forearm muscle studied by 31P magnetic resonance spectroscopy. *J Physiol* 535: 901-928, 2001.
19. **Kemp GJ, Thompson CH, Taylor DJ, and Radda GK**. Proton efflux in human skeletal muscle during recovery from exercise. *Eur J Appl Physiol Occup Physiol* 76: 462-471, 1997.
20. **Kingsley-Hickman PB, Sako EY, Mohanakrishnan P, Robitaille PM, From AH, Foker JE, and Ugurbil K**. 31P NMR studies of ATP synthesis and hydrolysis kinetics in the intact myocardium. *Biochemistry* 26: 7501-7510, 1987.
21. **LaNoue KF, Jeffries FM, and Radda GK**. Kinetic control of mitochondrial ATP synthesis. *Biochemistry* 25: 7667-7675, 1986.
22. **Laurent D, Yerby B, Deacon R, and Gao J**. Diet-induced modulation of mitochondrial activity in rat muscle. *Am J Physiol Endocrinol Metab* 293: E1169-1177, 2007.
23. **Naressi A, Couturier C, Devos JM, Janssen M, Mangeat C, de Beer R, and Graveron-Demilly D**. Java-based graphical user interface for the MRUI quantitation package. *MAGMA* 12: 141-152, 2001.
24. **Newcomer BR, and Boska MD**. T1 measurements of 31P metabolites in resting and exercising human gastrocnemius/soleus muscle at 1.5 Tesla. *Magn Reson Med* 41: 486-494, 1999.
25. **Phillips AC, Sleigh A, McAllister CJ, Brage S, Carpenter TA, Kemp GJ, and Holland AJ**. Defective mitochondrial function in vivo in skeletal muscle in adults with Down's syndrome: a 31P-MRS study. *PLoS One* 8: e84031, 2013.
26. **Portman MA**. Measurement of unidirectional Pi->ATP flux in lamb myocardium in-vivo. *Biochimica Et Biophysica Acta-Bioenergetics* 1185: 221-227, 1994.
27. **Prompers JJ, Wessels B, Kemp GJ, and Nicolay K**. MITOCHONDRIA: investigation of in vivo muscle mitochondrial function by 31P magnetic resonance spectroscopy. *Int J Biochem Cell Biol* 50: 67-72, 2014.
28. **Romijn JA, Coyle EF, Sidossis LS, Gastaldelli A, Horowitz JF, Endert E, and Wolfe RR**. Regulation of endogenous fat and carbohydrate metabolism in relation to exercise intensity and duration. *Am J Physiol* 265: E380-391, 1993.
29. **Schmid AI, Schrauwen-Hinderling VB, Andreas M, Wolzt M, Moser E, and Roden M**. Comparison of measuring energy metabolism by different 31P-magnetic resonance spectroscopy techniques in resting, ischemic, and exercising muscle. *Magn Reson Med* 67: 898-905, 2011.
30. **Sheldon JG, Williams SP, Fulton AM, and Brindle KM**. 31P NMR magnetization transfer study of the control of ATP turnover in Saccharomyces cerevisiae. *Proc Natl Acad Sci U S A* 93: 6399-6404, 1996.
31. **Shonk CE, and Boxer GE**. Enzyme Patterns in Human Tissues .I. Methods for Determination of Glycolytic Enzymes. *Cancer Research* 24: 709-721, 1964.
32. **Shonk CE, Boxer GE, Majima H, and Koven BJ**. Enzyme Patterns in Human Tissues .2. Glycolytic Enzyme Patterns in Nonmalignant Human Tissues. *Cancer Research* 24: 722-731, 1964.
33. **Sleigh A, Raymond-Barker P, Thackray K, Porter D, Hatunic M, Vottero A, Burren C, Mitchell C, McIntyre M, Brage S, Carpenter TA, Murgatroyd PR, Brindle KM, Kemp GJ, O'Rahilly S, Semple RK, and Savage DB**. Mitochondrial dysfunction in patients with primary congenital insulin resistance. *J Clin Invest* 121: 2457-2461, 2011.
34. **Tannus A, and Garwood M**. Adiabatic pulses. *NMR Biomed* 10: 423-434, 1997.

35. **van den Broek NM, Ciapaite J, Nicolay K, and Prompers JJ**. Comparison of in vivo postexercise phosphocreatine recovery and resting ATP synthesis flux for the assessment of skeletal muscle mitochondrial function. *Am J Physiol Cell Physiol* 299: C1136-1143, 2010.
36. **Vanhamme L, van den Boogaart A, and Van Huffel S**. Improved method for accurate and efficient quantification of MRS data with use of prior knowledge. *J Magn Reson* 129: 35-43, 1997.
37. **Yerby B, Deacon R, Beaulieu V, Liang J, Gao J, and Laurent D**. Insulin-stimulated mitochondrial adenosine triphosphate synthesis is blunted in skeletal muscles of high-fat-fed rats. *Metabolism* 57: 1584-1590, 2008.

Figure 1. Schematic representation of the ^{31}P-MRS exercise protocol

Solid lines symbolize sequence blocks and the grey shaded regions correspond to when exercise occurred. Time from onset of exercise is illustrated by the timeline. In the first exercise section, once exercising steady state conditions were met, spectra were obtained with saturation of the γ-ATP resonance and then control saturation placed equidistant to the Pi resonance (SAT-CONT expts). Spectra were also obtained with a long TR of 44s for calculation of metabolite concentrations (METAB). Following exercise cessation a phosphocreatine (PCr) recovery measurement (REC) was used to assess the immediate end of exercise oxidative ATP synthesis rate. Within the second exercise, once in steady state, the inversion recovery data were acquired with varying TI's (IR expts) with an effective TR of 6s, and a measure of Mo was also obtained. The four stars represent comparison sites for steady state conditions.

Figure 2. Individual timecourse of metabolite concentrations obtained during steady state exercise with alternating γ-ATP and control irradiation.

Representative (group B volunteer) metabolite concentration timecourse of phosphocreatine (PCr, squares), inorganic phosphate (Pi, circles) and γ-ATP (triangles), obtained during steady state exercise conditions with alternating frequency of saturation (SAT-CONT section in Figure 1). Each x-axis point corresponds to a single spectrum. Even scan numbers correspond to spectra obtained with saturation of γ-ATP (SAT) and odd scan numbers to the equivalent control saturation frequency equidistant to Pi (CONT). Consecutive points are joined by grey dashed (PCr), solid black (Pi), and dotted black (γ-ATP) lines to aid visualization.

549 Figure 3. ^{31}P-MRS measurements of Pi->ATP flux at rest and during steady state exercise.

550 Representative ST spectra at rest (A) and during steady state exercise (C), with saturation of
551 the γ-ATP resonance (SAT) (right, lower A,C) and corresponding control spectrum (CONT)
552 (right, upper A,C). The CONT spectra show the phosphomonoester (PME), Pi, and
553 phosphodiester (PDE) resonances (left A,C), superimposed with the SAT Pi resonance to
554 show the difference (Δ) in the Pi resonance. Corresponding inversion recovery plot for
555 measurement of the Pi T_1 in the presence of γ-ATP saturation, both at rest (B) and during
556 steady state exercise (D).

557

558

559

560 Figure 4. Steady state rates of exercising Pi->ATP flux and its increment above basal levels,
561 compared with measures of oxidative ATP synthesis rates

562 Exercising steady state rates of Pi->ATP flux ($V_{Pi\text{-}ATP}$) (A) and its increment above basal
563 levels (B), plotted against oxidative ATP synthesis rates (V_{ATP}) as measured from the
564 immediate end of exercise PCr resynthesis rate. Black stars represent the individuals in group
565 A, and the multiple scans of the three volunteers in group B are denoted by circles of black,
566 grey and white respectively. The solid line represents unity equivalence of the two rates.

567

568

569

Figure 5. Paired-samples difference (Δ) in surplus Pi->ATP flux and substrate concentrations of the enzymes GAPDH and PGK between steady state exercise and resting conditions.

Paired-samples (n = 9) mean difference ± SEM (exercising – resting values) for surplus V_{Pi-ATP} and substrate concentrations of the enzymes GAPDH and PGK; inorganic phosphate (Pi), adenosine diphosphate (ADP), and hydrogen ions (H^+). Surplus V_{Pi-ATP} was calculated by subtracting the net rate of oxidative ATP synthesis, V_{ATP}, (estimated as the immediate post-exercise PCr resynthesis rate) from the rate of Pi->ATP flux during exercise (V_{Pi-ATP}), to provide an estimate of the component of the ST measurement not explained by suprabasal mitochondrial ATP synthesis. Data from group B have been averaged to provide one value per person to avoid inappropriate weighting (hence n = 9). A paired-samples t-test was used to test for significant differences between resting and exercising conditions (p-values shown).

590

591 Figure 6. Relationship of the Pi->ATP flux with the concentration of phosphomonoester
592 PME, at rest and during steady-state exercise

593 A) Correlation of resting Pi->ATP flux ($V_{Pi\text{-}ATP}$) with resting [PME] ($r = 0.740$, $p<0.001$, $n =$
594 18), and B) relationship of exercising $V_{Pi\text{-}ATP}$ with exercising [PME] ($r = 0.730$, $p = 0.001$, $n =$
595 18). As in Figure 4: Black stars represent the individuals in group A, and the multiple scans of
596 the three volunteers in group B are denoted by circles of black, grey and white respectively.

597 C) Surplus $V_{Pi\text{-}ATP}$ relative to [PME] at rest (white diamonds, $n = 18$) and during exercise
598 (grey and black diamonds, $n = 18$). Surplus $V_{Pi\text{-}ATP}$ was calculated by subtracting the rate of
599 suprabasal oxidative ATP synthesis, V_{ATP}, (estimated as the immediate post-exercise PCr
600 resynthesis rate) from the exercising $V_{Pi\text{-}ATP}$. Resting $V_{Pi\text{-}ATP}$ alone was used for the equivalent
601 measure in resting muscle, where suprabasal ATP synthesis is by definition zero. Linear
602 regression using both resting and exercising data ($n = 36$) found that in addition to [PME],
603 V_{ATP} was also a significant negative predictor of surplus $V_{Pi\text{-}ATP}$ (both [PME] and V_{ATP}
604 $p<0.001$). This is illustrated schematically here by dividing the exercising data into low (0.0 –
605 14.9 mM/min) and high (15.0 – 30.5 mM/min) exercising V_{ATP} groups, denoted by grey and
606 black diamonds respectively. To aid visualization the dashed and solid black lines represent
607 the trendlines for rest and high exercising V_{ATP} groups respectively, and highlight the
608 association of V_{ATP} with reductions in the surplus $V_{Pi\text{-}ATP}$ for a given [PME].

609

610

611

612

613 Table 1. Mean resting and exercising ST and PCr resynthesis measures.

	Resting	Exercising	* Paired-samples difference	** p-value
ST (n=9)				
[Pi] (mM)	3.37 ± 0.18	10.23 ± 1.10	6.9 ± 1.1	<0.001
T_1' (s)	4.5 ± 0.1	4.8 ± 0.3	0.3 ± 0.3	0.376
k' (min^{-1})	2.98 ± 0.35	2.44 ± 0.16	-0.54 ± 0.39	0.204
V_{Pi-ATP} (mM/min)	9.8 ± 0.9	25.0 ± 2.9	15.1 ± 3.5	0.003
PCr resynthesis (n=11)				
[PCr] (mM)	32.9 ± 1.0	23.5 ± 1.2	- 9.3 ± 1.2	<0.001
V_{ATP} (mM/min)	†	16.5 ± 1.8		ND

614

615 Data presented are mean ± SEM. Data from group B have been averaged to provide one value
616 per person to avoid inappropriate weighting. * Paired-samples difference (exercising –
617 resting). ** Paired samples t-test to test for significant differences between rest and exercising
618 conditions. † For comparison with exercising this is 0.0 as V_{ATP} reflects suprabasal oxidative
619 ATP synthesis. The net rate of basal oxidative ATP turnover is thought to be approximately
620 0.5 mM/min (16).

621

622 T_1', apparent longitudinal relaxation time of Pi in the presence of saturation of the γ-ATP
623 resonance; k', first order rate constant; V_{Pi-ATP}, rate of Pi->ATP flux; [PCr], concentration of
624 phosphocreatine; V_{ATP}, suprabasal oxidative rate of ATP synthesis determined from
625 immediate end of exercise PCr resynthesis; ND, not determined.

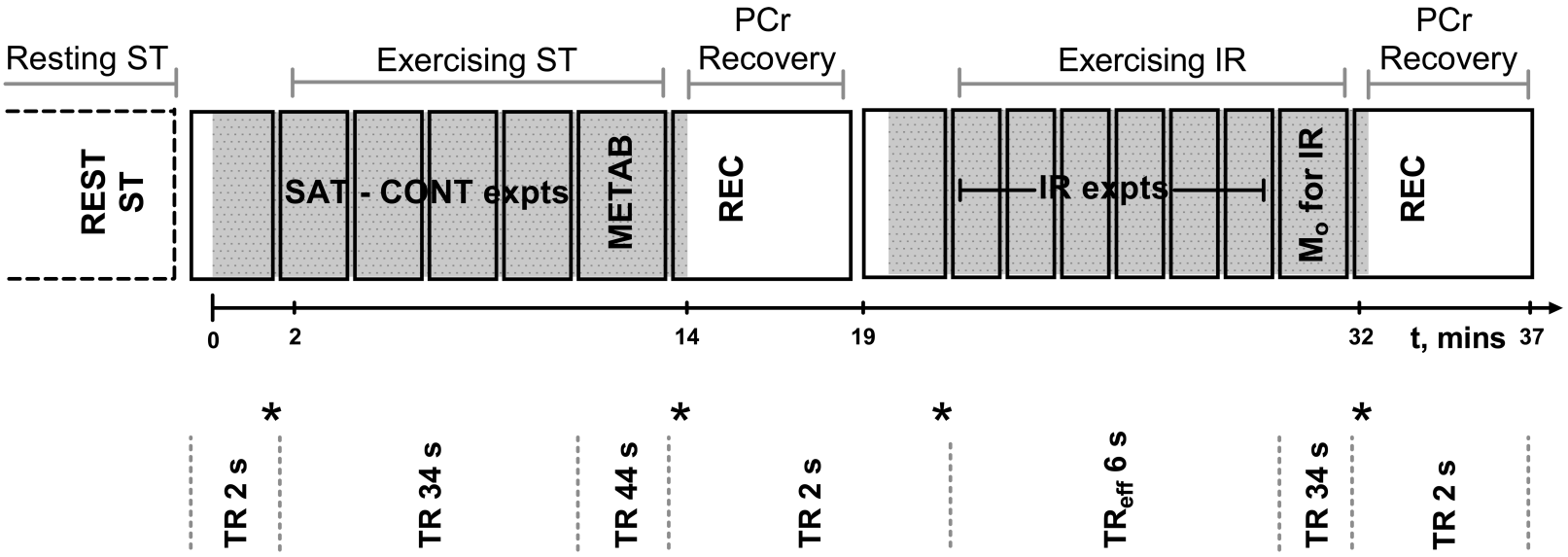
Resting ST
Exercising ST
PCr Recovery
Exercising IR
PCr Recovery
REST ST
SAT - CONT expts
METAB
REC
IR expts
M_o for IR
REC
0
2
14
19
32
t, mins
37
TR 2 s
TR 34 s
TR 44 s
TR 2 s
TR_{eff} 6 s
TR 34 s
TR 2 s

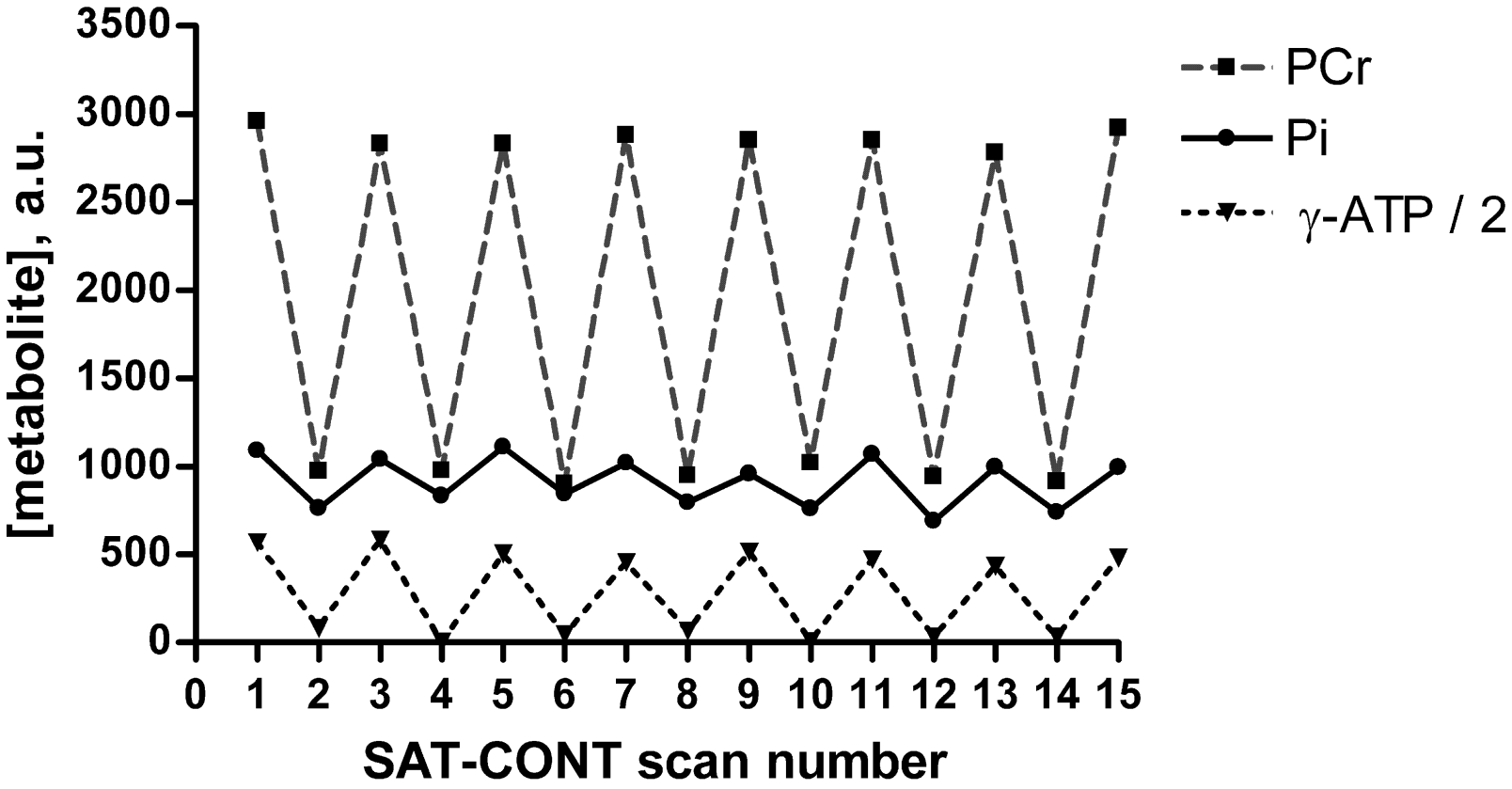
3500
3000
2500
2000
1500
1000
500
0
[metabolite], a.u.
0 1 2 3 4 5 6 7 8 9 10 11 12 13 14 15
SAT-CONT scan number
PCr
Pi
γ-ATP / 2

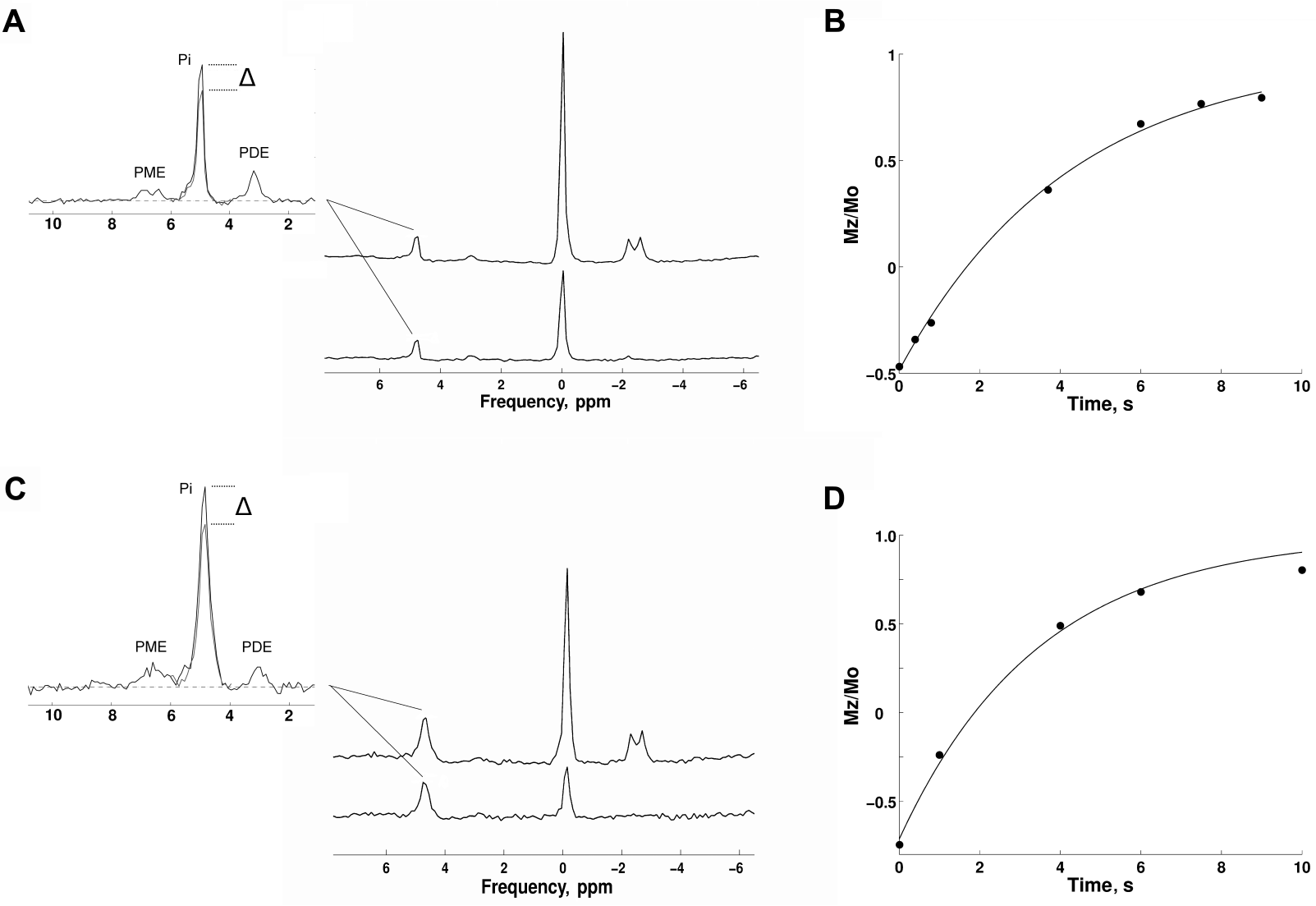
A
Pi
Δ
PME
PDE
10
8
6
4
2
6
4
2
0
−2
−4
−6
Frequency, ppm
B
1
0.5
0
−0.5
Mz/Mo
0
2
4
6
8
10
Time, s
C
Pi
Δ
PME
PDE
10
8
6
4
2
6
4
2
0
−2
−4
−6
Frequency, ppm
D
1.0
0.5
0
−0.5
Mz/Mo
0
2
4
6
8
10
Time, s

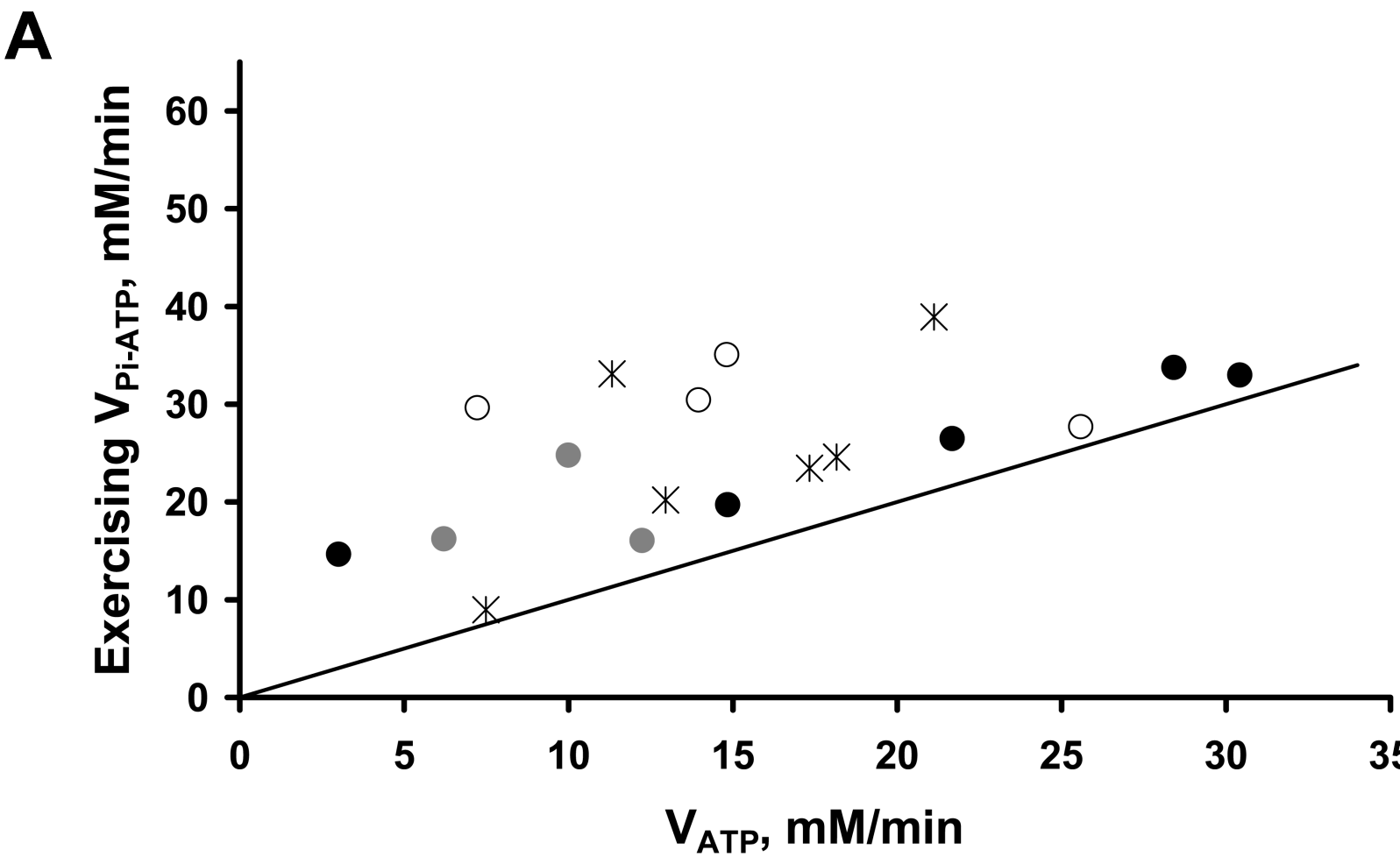
A
Exercising V_{Pi-ATP}, mM/min
60
50
40
30
20
10
0
0
5
10
15
20
25
30
35
V_{ATP}, mM/min

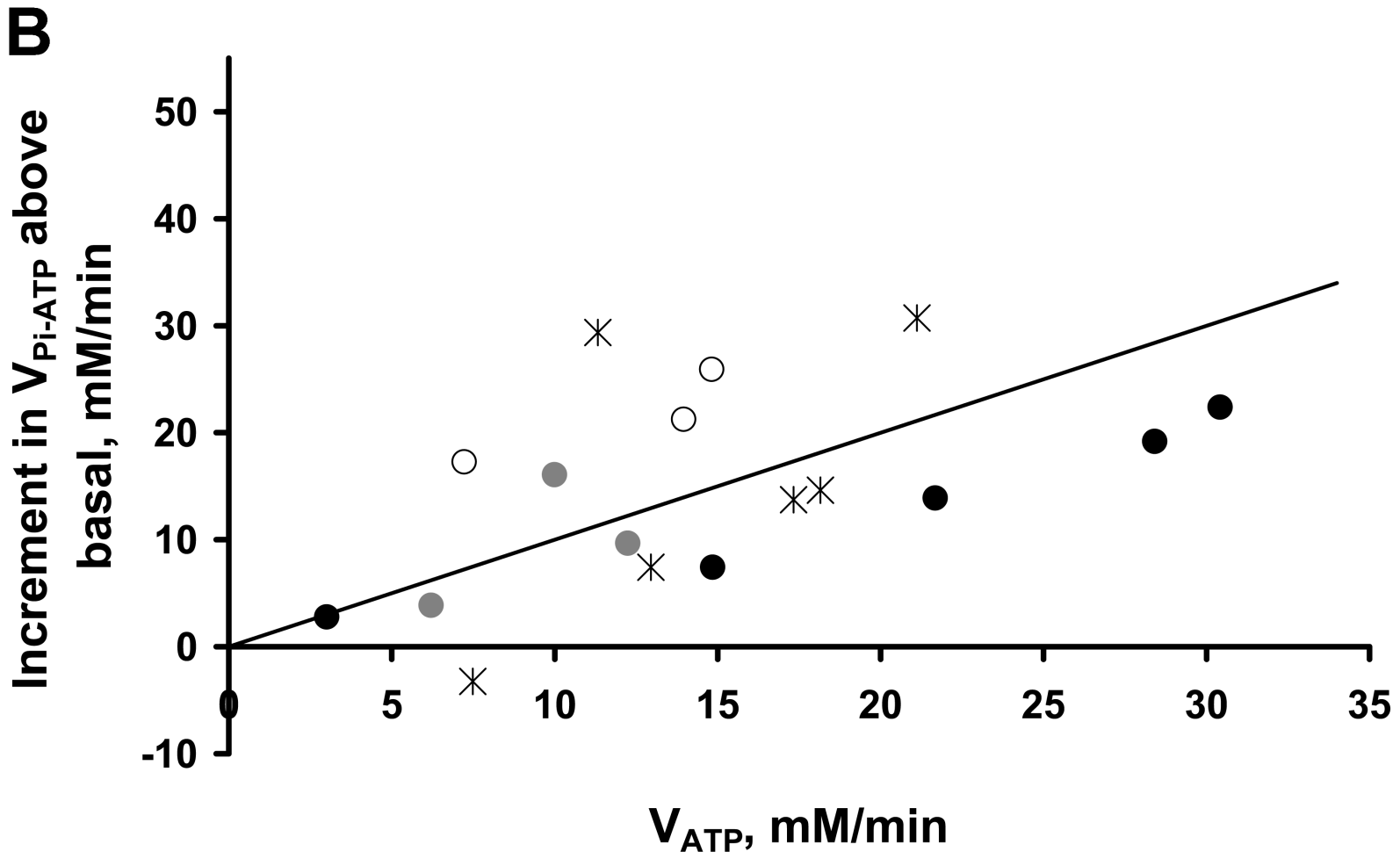
B
Increment in V_{Pi-ATP} above basal, mM/min
50
40
30
20
10
0
-10
0
5
10
15
20
25
30
35
V_{ATP}, mM/min

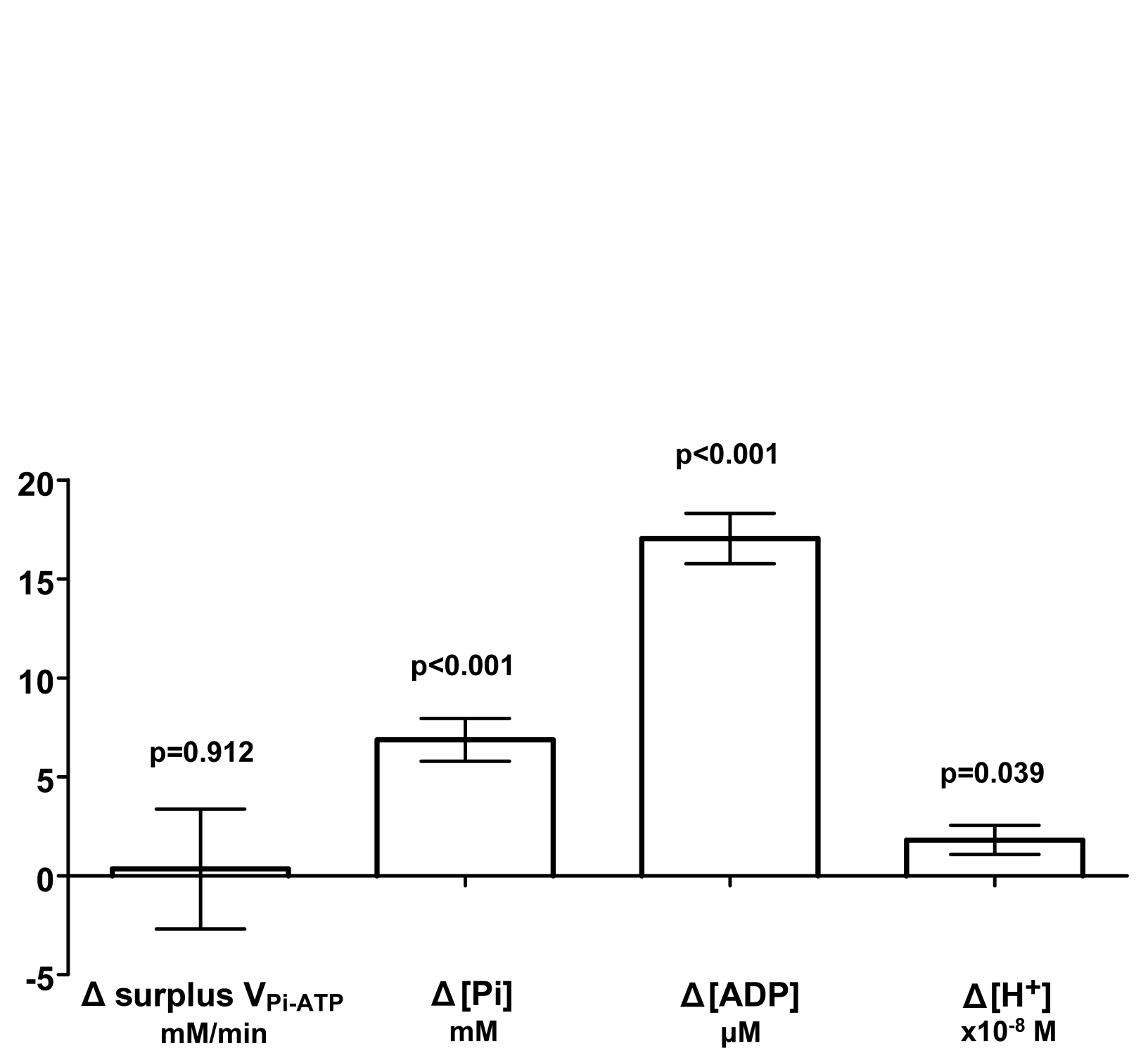
p<0.001
20
15
p<0.001
10
p=0.912
5
p=0.039
0
-5
Δ surplus V Pi-ATP
mM/min
Δ [Pi]
mM
Δ [ADP]
μM
Δ [H+]
x10-8 M

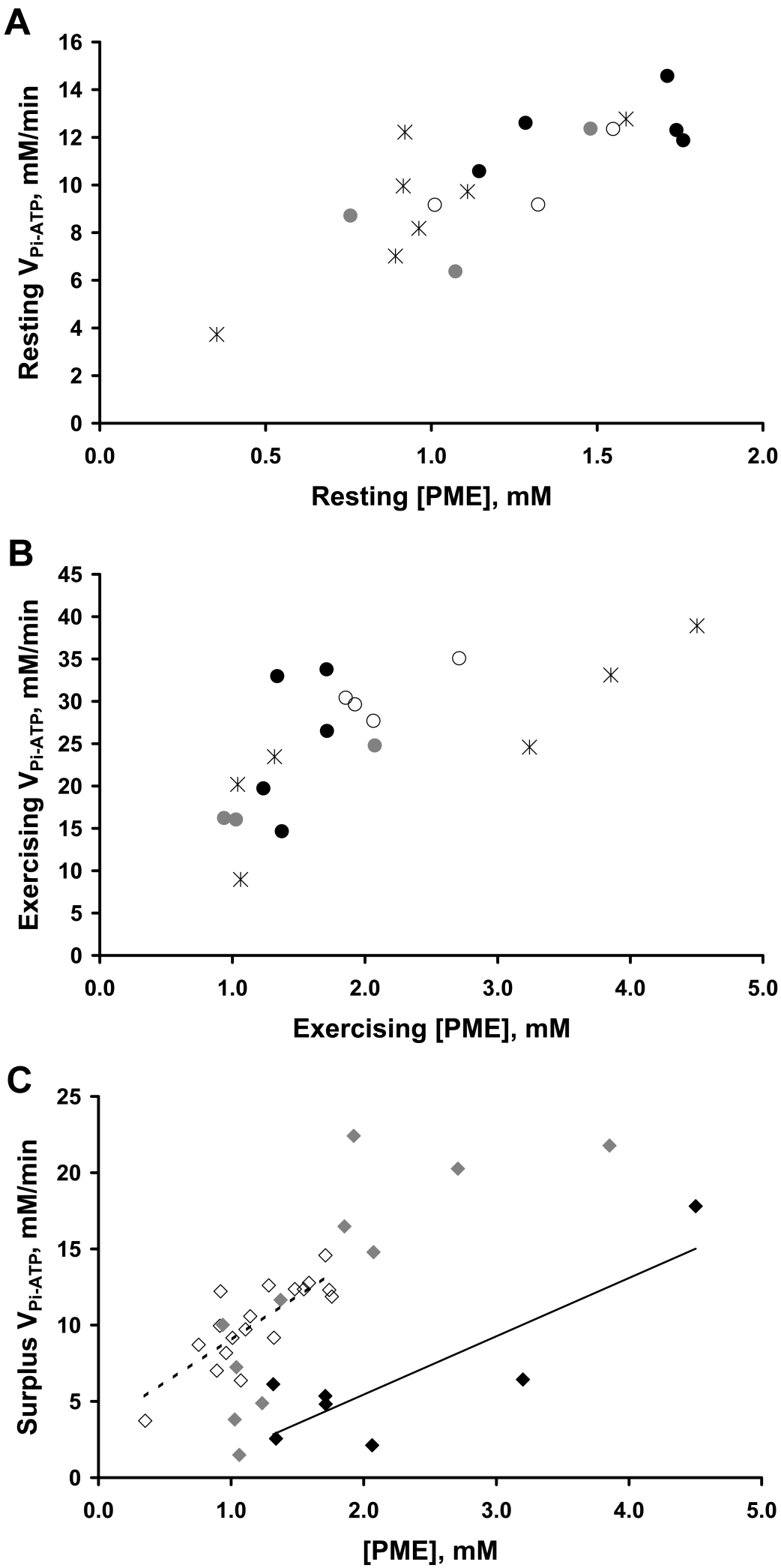
A
Resting V_{Pi-ATP}, mM/min
Resting [PME], mM
B
Exercising V_{Pi-ATP}, mM/min
Exercising [PME], mM
C
Surplus V_{Pi-ATP}, mM/min
[PME], mM